GNPy: An open source application for physical layer aware open optical networks

JOURNAL OF
Optical Communications
and Networking

GNPy: an open source application for physical layer aware open optical networks

Alessio Ferrari,[1,*] Mark Filer,[2] Karthikeyan Balasubramanian,[2] Yawei Yin,[2] Esther Le Rouzic,[3] Jan Kundrát,[4] Gert Grammel,[5] Gabriele Galimberti,[6] and Vittorio Curri[1]

[1]DET, Politecnico di Torino, Corso Duca degli Abruzzi 24, Torino (TO) 10129, Italy
[2]Microsoft Corporation, Redmond, Washington 98052, USA
[3]Orange Labs, 22300 Lannion, France
[4]CESNET, Prague, Czech Republic
[5]Juniper Networks, Stuttgart, Germany
[6]Cisco Photonics, via S. M. Molgora, 48/C, Vimercate (MI), 20871, Italy
*Corresponding author: alessio.ferrari@polito.it

Received 13 November 2019; revised 20 February 2020; accepted 20 February 2020; published 16 March 2020 (Doc. ID 382906)

In this paper, we describe the validation of GNPy. GNPy is an open source application that approaches the optical layer according to a disaggregated paradigm, and its core engine is a quality-of-transmission estimator for coherent wavelength division multiplexed optical networks. This software is versatile. It can be used to prepare a request for proposal/request for quotation, as an engine of a what-if analysis on the physical layer, to optimize the network configuration to maximize the channel capacity, and to investigate the capacity and performance of a deployed network. We validate GNPy by feeding it with data from the network controller and comparing the results to experimental measurements on mixed-fiber, Raman-amplified, multivendor scenarios over the full C-band. We then test transmission distances from 400 up to 4000 km, polarization-multiplexed (PM) quadrature phase shift keying, the PM-8 quadrature amplitude modulation (QAM) and PM-16QAM formats, erbium-doped fiber amplifier (EDFA) and mixed Raman–EDFA amplification, and different power levels. We show excellent accuracy in predicting both the optical signal-to-noise ratio and the generalized signal-to-noise ratio (GSNR), within 1 dB accuracy for more than 90% of the 500 experimental samples. We also demonstrate the ability to estimate the transmitted power maximizing the GSNR within 0.5 dB of accuracy.

https://doi.org/10.1364/JOCN.382906

1. INTRODUCTION

Network operators are interested in maintaining the best performance of their optical networks and identifying potential performance bottlenecks. However, it is hard to have a unified vendor-neutral performance map of the optical network because every vendor uses different performance prediction methods and performance indicators. This creates artificial barriers for operators, since expressing performance expectations in a request for proposal/request for quotation (RFP/RFQ) process can become vendor dependent. Operators need a tool to quickly model an optical network and run simulations in a vendor-neutral manner to properly match their expectations with an implementation. In particular, such a vendor-neutral simulation would allow the seamless carryover of data from the past and from different vendors when modeling new networks. Breaking through the barrier, in 2017 the Open Optical & Packet Transport–Physical Simulation Environment (OOPT–PSE) group within the Telecom Infra Project (TIP) [1] started to define and develop a common, open source, and vendor-neutral set of algorithms to assess the optical impairments in an open optical line system.

The core software developed by the OOPT–PSE team is called Gaussian noise simulation in Python (GNPy) [2]. It relies on a quality-of-transmission (QoT) estimator that, given the network status, calculates the generalized signal-to-noise ratio (GSNR) [3] over a described network route. Furthermore, applications have been developed to describe [4], design [5,6], and optimize [7,8] optical networks based on it. In essence, it allows a user to determine the feasibility of modulation and capacity allocation in a fully coherent wavelength division multiplexed (WDM) network with vendor-independent software. The computational time is a few seconds per lightpath (LP), with a future target of well below one second per LP.

In past experiments, GNPy has been used with excellent results in deployed networks, such as in 2017 [9,10]. However,

those experiments did not validate GNPy's capability of QoT prediction on the entire C-band with Raman amplification and did not benefit from a quasi-automatic procedure to provide input from the network controller directly to GNPy.

In this paper, we extend the description in [11] by expanding the previously obtained results. We also provide a detailed description of the methodology to obtain reliable estimations from GNPy in a real network. In doing so, GNPy used the data structure provided by the network controller, including power levels measured by the on-board photodiodes and complemented it with data provided by the documentation of devices such as the gain versus noise figure (NF) characterization of the amplifiers. Hence, to the best of our knowledge, this is the first validation of the entire process from data collection to the actual performance estimation. We believe it proves the feasibility of GNPy integration in a network automation framework to enable operations such as path computation for automatic lightpath deployment and recovery. The validation process compared the estimated QoT, captured by the GSNR, against measurements.

This paper has five sections. In Section 2, we depict the general structure of GNPy and detail the core of GNPy: the QoT estimator calculating the GSNR. In Section 3, we describe the methodology used to validate the QoT estimation. This procedure can also be used as a guide to feed GNPy with adequate network parameters. Then, in Section 4, we describe the testbed and present the validation results. Finally, in Section 5 we draw conclusions and address the future evolution.

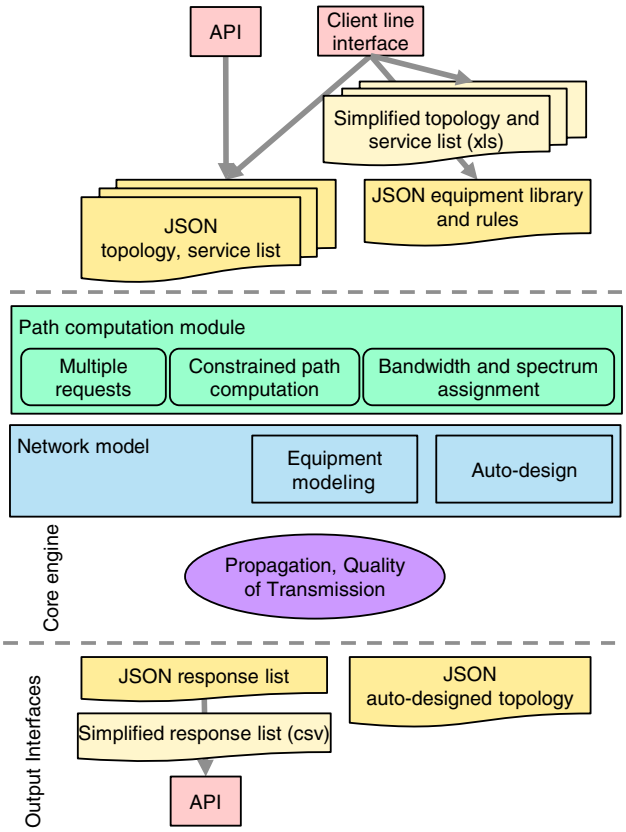

Fig. 1. GNPy general structure.

2. GNPy: STRUCTURE AND IMPLEMENTATION

The general GNPy structure is illustrated in Fig. 1. GNPy provides a set of features structured around a core engine that takes care of propagation effects and the QoT estimation. The core engine is usually configured to simulate the propagation of a fully loaded spectrum between points A and B in a complex topology. The network is built from atomic network elements, such as the erbium-doped fiber amplifier (EDFA) and the fiber. As a result of the simulation, the core returns the GSNR [3] for each channel along the path. The GSNR has been proven as an effective unique metric for the QoT for modern coherent multilevel-modulated uncompensated WDM optical transmission [10].

More advanced features are handled by add-on modules that call out to the core engine for point-to-point QoT estimations.

To have meaningful GSNR results, GNPy requires a set of input parameters for each of the network elements along the path. In stable releases, these parameters are provided either in JavaScript object notation (JSON) format, or as a set of Microsoft Excel files that are internally mapped into an equivalent JSON structure. Together, the parameters are used as inputs to calculate the amplified spontaneous emission (ASE) noise and the nonlinear interference (NLI) disturbance generated by the nonlinear fiber propagation.

As a source of noise contribution toward the GSNR, the ASE noise depends strongly on the particular EDFA model. Amplifiers are described according to three general models [12], depending on the amount of knowledge of the amplifier:

1. A detailed white-box model that permits a user to define precise NF versus gain for open devices whenever access to detailed performance is possible.
2. An operator model that represents proprietary equipment for which knowledge is limited to a small amount of NF-gain values, available in data sheets.
3. A black-box model, for which key attributes, such as internal output attenuation or switched gain range, are not available.

The capability to support different amplifier models is a key enabler for a multivendor application. Based on this equipment model, a user can model a given green- or brown-field configuration, provided that the whole set of equipment attributes is available.

There are scenarios when such a precise description is not available. For this reason, GNPy offers an auto-design feature that can determine the amplifier configuration for a possible deployment on the basis of a set of design rules and heuristics. This practical implementation of optimization strategies is proposed in [12].

In auto-design mode, the input topology is not complete. The spans are not necessarily specified with all amplifiers, and the amplifier model and their operating points are not specified. Auto-design instead picks suitable amplifiers from the equipment library and automatically splits long fiber spans.

A set of features eases the user experience for planning and what-if scenarios: It enables the propagation of multiple requests on the same simulated network (i.e., the same

configuration of equipment). Typical planning constraints are supported, such as path disjunction, mandatory nodes to be crossed, spectrum assignment, and transponder mode selection. This planning requires a third input from the user, listing the set of requests to be evaluated with their constraints. The interface to this feature is a JSON file whose structure is inspired by [4]. This path computation module enables the development of an application program interface (API) for integration with optical line system controllers. For example, this API was recently featured at the 2019 TIP Summit in an open disaggregated transport network (ODTN) demonstration with the Czech Light Open Line System [13]. The path feasibility estimation also has been delegated to GNPy in the Sodium Stability Release 2 (Sodium-SR2) of the TransportPCE project [14].

The QoT estimator of GNPy requires a description of the network through a JSON file. It is abstracted as an optical impairment-aware topology [4,15] (Fig. 2) in which each network element is properly connected to the others, and it returns the GSNR for each channel at the end of a path. A network element can be a fiber, an optical amplifier, a reconfigurable optical add-drop multiplexer (ROADM) node, or a transceiver. Given this description of the physical layer, the GSNR between a source transceiver and a destination transceiver is assessed through the path under analysis by using the so-called spectral information. The aim of the spectral information is to maintain all of the information related to the WDM comb, such as the power of each channel, the roll-off, the symbol rate, the central frequency, the amount of ASE noise, and NLI that affects that channel. Thus, such spectral information is generated by the source transceiver and it is propagated through each network element belonging to the path under analysis. These network elements update the spectral information by properly attenuating or amplifying each power value and by adding new ASE and NLI noise contributions on the spectral information if it is warranted. In particular, a ROADM node may add some noise in the add/drop channels and it equalizes the power per channel of the spectral information. The amplifier properly amplifies the spectral information and introduces some new ASE noise, taking into account the possible frequency variation of the gain and the NF. The ASE noise power contribution, as a function

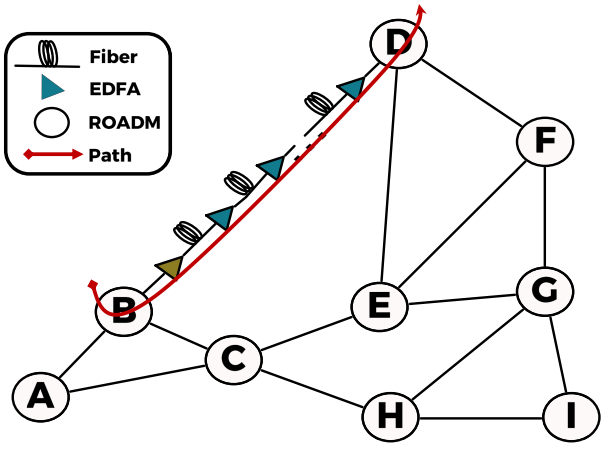

Fig. 2. Path propagation in GNPy to assess the QoT.

of the frequency f, is computed as

$$P_{\mathrm{ASE}}(f) = hf\mathrm{NF}(f)G(f)B_{\mathrm{ref}}, \tag{1}$$

where h is the Planck constant, $G(f)$ is the amplifier gain, and B_{ref} is the reference bandwidth in which the GSNR is evaluated. The fiber propagation attenuates the power levels and properly introduces the NLI generated by the Kerr effect, also taking into account the stimulated Raman scattering (SRS) [16–19].

The SRS is assessed by implementing a Raman solver that numerically computes the solution of the set of ordinary differential equations (ODEs) that describe the SRS effect, also including the two-point boundary value problem in the presence of counter-propagating Raman pumps, as shown in [20]. Thanks to the Raman solver, it is possible to assess the interchannel SRS, the SRS excited by the presence of co- and counter-propagating Raman pumps generated by Raman amplifiers, and also the spontaneous Raman scattering that is fundamental to assess the ASE noise generated by Raman amplifiers. Then, the NLI contribution of each fiber span is treated as an additive white Gaussian noise disturbance that takes into account the SRS according to the generalized Gaussian noise (GGN) model [16–19]. This contribution is evaluated as

$$P_{\mathrm{NLI}}(f) = G_{\mathrm{NLI}}(f)B_{\mathrm{ref}}, \tag{2}$$

where $G_{\mathrm{NLI}}(f)$ is the NLI power spectral density, which depends on the fiber parameters and on the WDM spectral occupancy. $G_{\mathrm{NLI}}(f)$ is decomposed into self-channel interference (SCI), cross-channel interference (XCI), and multichannel interference (MCI). While the SCI and the XCI are computed via the GGN model, the multichannel interference (MCI) is not computed because it is negligible [21,22]. This reduces the computational time as the complexity of the problem moves from quadratic with respect to the number of channels to linear. Finally, the transceiver at the end of the path receives the spectral information and returns the propagation performances of each channel by computing the GSNR, which includes both the optical signal-to-noise ratio (OSNR) and the nonlinear signal-to-noise ratio ($\mathrm{SNR_{NL}}$). Those quantities are defined and computed on the ith channel as

$$\mathrm{OSNR}_i = \frac{P_{S,i}}{P_{\mathrm{ASE}}(f_i)}, \tag{3}$$

$$\mathrm{SNR}_{\mathrm{NL,i}} = \frac{P_{S,i}}{P_{\mathrm{NLI}}(f_i)}, \tag{4}$$

$$\mathrm{GSNR}_i = \frac{P_{S,i}}{P_{\mathrm{ASE}}(f_i) + P_{\mathrm{NLI}}(f_i)} = \left(\mathrm{OSNR}_i^{-1} + \mathrm{SNR}_{\mathrm{NL,i}}^{-1}\right)^{-1}, \tag{5}$$

where $P_{S,i}$ is the signal power of the ith channel and f_i is its central frequency.

3. VALIDATION METHODOLOGY

The aim of this validation is to prove the capability of GNPy to predict the GSNR of real commercial line systems, relying

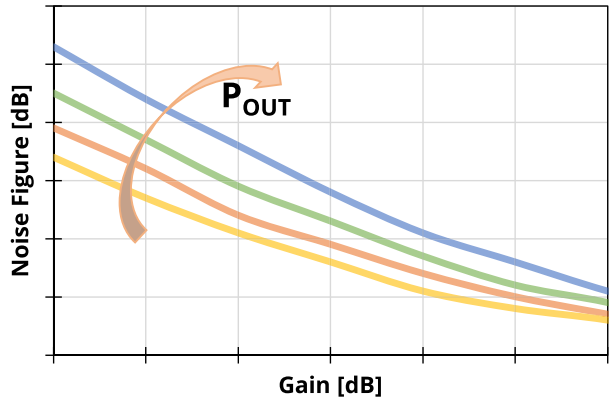

Fig. 3. Qualitative example of the noise-figure-versus-gain and P_{out} curves of an amplifier.

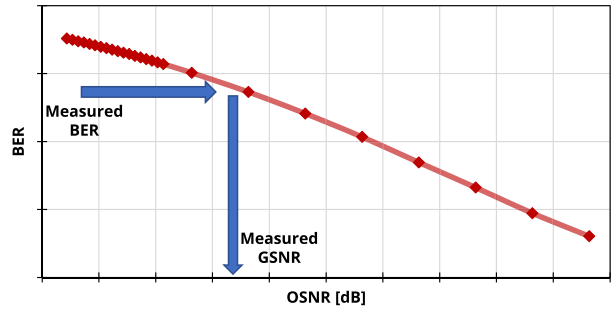

Fig. 4. Qualitative example of the B2B BER-versus-OSNR response of the transponder and derivation of the GSNR from a BER measurement.

only on data provided by the network equipment, such as the power levels measured by the on-board photodiodes and the parameters, such as the gain-versus-NF characterization of the EDFAs, provided by the documentation of the devices. Hence, in this section, we describe this process, which leads to the building of the JSON that describes ROADM nodes, fibers, and amplifiers.

Each ROADM node requires a target output power per channel that can be retrieved from the total power measured by the photodiode before the booster amplifier divided by the number of channels. Then, each amplifier requires a gain target and a tilt target, and this information can be provided by the network equipment. The information then can be retrieved with a representational state transfer (REST) [23] query or other methods, such as using network configuration protocol (NETCONF) [24] directly on the equipment, can be adopted. Furthermore, the amplifier NF must be derived to properly assess the ASE noise level. To do this, the data model of GNPy for EDFA is fed with the gain-versus-NF characterization from the documentation of the amplifier. Because this curve also depends on the input power, it is necessary to use the proper curve, depending on the output power (P_{out}) level that is measured by the amplifier photodiode. A qualitative example of NF-versus-gain and P_{out} characterization is shown in Fig. 3. The values in Fig. 3 are for illustration purposes only and not from any real amplifier.

To describe a fiber span, it is necessary to input the fiber type, the fiber length (L_F), the attenuation coefficient (α), and the connector losses. Furthermore, when Raman pumps are injected into the fiber by Raman amplifiers, the parameters related to the Raman pumps and the temperature of the fiber also are needed. The fiber types already available in GNPy are standard single-mode fiber (SSMF), nonzero dispersion-shifted fiber (NZDSF), and large effective area fiber (LEAF). It also is possible to define custom fiber types. To define a custom fiber type, it is enough to know the dispersion, the nonlinear coefficient, and the Raman efficiency. The length L_F can be retrieved by computing the distance between the locations of the amplification sites or it can be obtained by the network equipment by measuring the propagation time between two amplifiers. For each fiber type we use the specified attenuation coefficient from the data sheet. Then, the connector losses can be estimated if you know the overall span loss (A_s): It can be derived by computing the difference between the total power measured by photodiodes placed at the output of the previous amplifier and at the input of the following amplifier. Thus, the overall splice-plus-connector loss (A_c) can be derived knowing A_s and the fiber loss (A_F), so

$$A_c = A_s - A_F = A_s - \alpha \times L_F. \tag{6}$$

The proper partition of this loss is crucial because the input connector loss determines the amount of NLI generated by that fiber span. As the optical time domain reflectometer (OTDR) trace is not always available, it may be impossible to retrieve the concentrated loss distribution along the fiber. For this reason, it is necessary to make some assumptions: For the input connector loss, we use 0.75 dB because it is a typical value reported in [25] and was used in [10,26]. The residual loss is then concentrated in the output connector loss even if the actual loss is distributed along the fiber because of the various splices. The fiber temperature, if not known, can simply be assumed to be equal to the 295 K room temperature.

Finally, the Raman pumps are described by their frequency and their power. The pump frequency is provided by the documentation, while the value of each transmitted pump power can be obtained from a REST query to the Raman amplifier. To properly derive the actual power of the pumps injected into the fiber, the output connector loss is subtracted. This value can be obtained by querying the OTDR situated on each Raman card.

By following this procedure for all the network elements, it is possible to complete the description of the topology, and GNPy can compute the QoT of a network path. In this procedure, we want to point out that the auto-design feature is not used.

To verify the accuracy of the estimation, it is necessary to measure the GSNR. We do it querying the bit error rate (BER) reported by the transponder and inferring the corresponding measured GSNR by inverting the back-to-back (B2B) BER-versus-OSNR characterization of the transponder, as qualitatively shown in Fig. 4. The values are not shown due to nondisclosure agreements with the manufacturer. We performed this procedure for each transceiver and for each modulation format. Finally, the error is computed as the difference between the measured GSNR and the one estimated by GNPy. We also observe the accuracy of predicting the OSNR

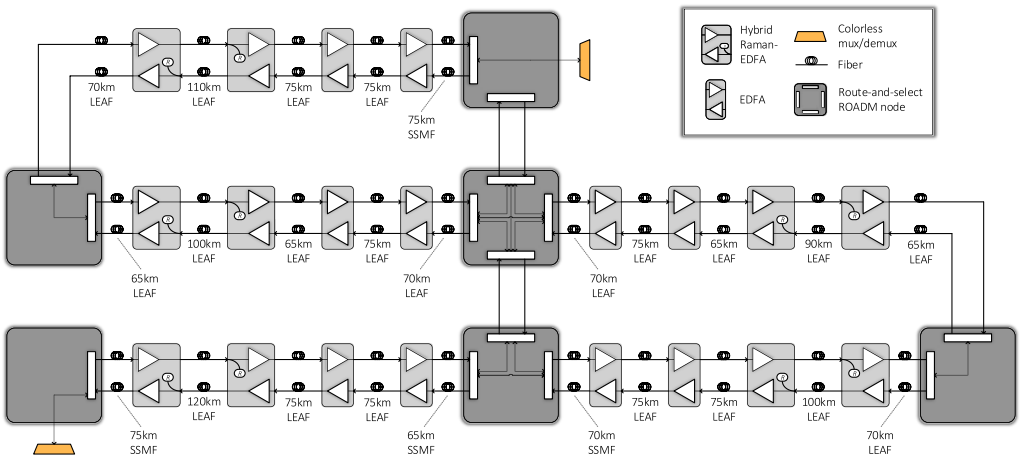

(a) Block scheme of the Microsoft testbed.

(b) A photo of the Microsoft testbed.

Fig. 5. (a) Block scheme and (b) photo of the Microsoft testbed.

by using the built-in functionality of the optical spectrum analyzer (OSA). As shown in [27], the signal and ASE noise power are estimated using an OSA. In particular, the ASE noise is estimated by measuring it at the left and right side of the channel and averaging the two measurements.

4. VALIDATION

In this section we describe the testbed used in Microsoft labs and report the validation results.

A. Testbed Description

The testbed used for the experiments is shown in Fig. 5: It emulates a commercial network with six ROADM nodes and five amplified optical segments, and the longest bidirectional path in the network is 2000 km long. The transponders come from three different vendors, whereas all the ROADM nodes and the amplifiers are from a fourth vendor. Each node degree of each ROADM node has a booster amplifier and a pre-amplifier. Each line segment is roughly 400 km long, and it includes four in-line amplifiers (ILA): three lumped EDFAs and one hybrid Raman–EDFA amplifier with Raman amplification operating in the moderate pumping regime [28]. The length of the fiber spans varies from 65 km to 120 km, and the fiber types are G.652 standard SSMF and G.655 LEAF. The exact network topology, including the detailed length of each fiber span, the fiber type, and the position of each EDFA and hybrid Raman–EDFA amplifier, is shown in Fig. 5(a). The line system has been properly configured by a vendor proprietary controller. To collect and prepare the information, as described in Section 3, the state of the network was probed by querying it using a Microsoft software-defined network (SDN) line system monitoring tool that is based on REST.

The normalized transmitted spectrum, shown in Fig. 6, is transmitted and received through a colorless mux/demux. Its bandwidth occupation is 4.7 THz, from 191.325 THz up to 196.025 THz. Commercial multivendor coherent transponders from three different vendors are used to generate a total

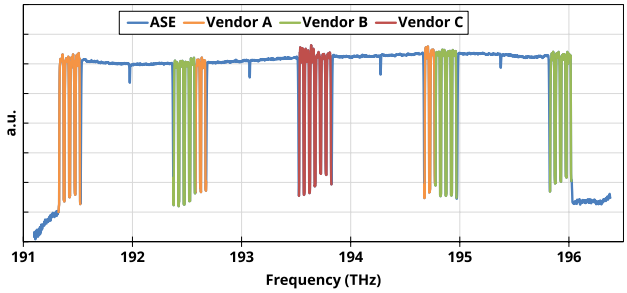

Fig. 6. Transmitted spectrum. Channels of different vendors are reported with different colors.

of 26 channels under test (CUTs), grouped into five media channels (MCs). Two MCs are composed of four channels, and the remaining three MCs are made up of six channels. The WDM grid spacing is 50 GHz. The MCs are distributed in the spectrum as follows: The two four-channel MCs are positioned at the edges of the spectrum, with one six-channel MC in the middle and the remaining two MCs at the midpoints between the central MC and the external MCs. The rest of the spectrum is filled with properly shaped ASE noise to obtain a full C-band spectral load, as shown in [29]. The signals are root-raised cosine shaped with a roll-off of 0.2, and the symbol rate is 34.16 GBaud. The transponders support three modulation formats: polarization-multiplexed (PM) quadrature phase shift keying (QPSK), PM-8 quadrature amplitude modulation (QAM), and PM-16QAM. We tested different modulation formats and propagation distances in forward and backward directions: PM-QPSK at 2000 km and 4000 km; PM-8QAM at 400 km, 800 km, 1200 km, 1600 km, and 2000 km; and PM-16QAM at 400 km, 800 km, and 1200 km. The 4000 km path was obtained by looping back the signals over the 2000 km path. Finally, we also tested PM-8QAM along the 2000 km path in both directions without Raman amplification. To do this, we turned off all the Raman amplifiers in all hybrid Raman–EDFA amplifiers and we set the gain of the EDFA to compensate for the absence of Raman gain.

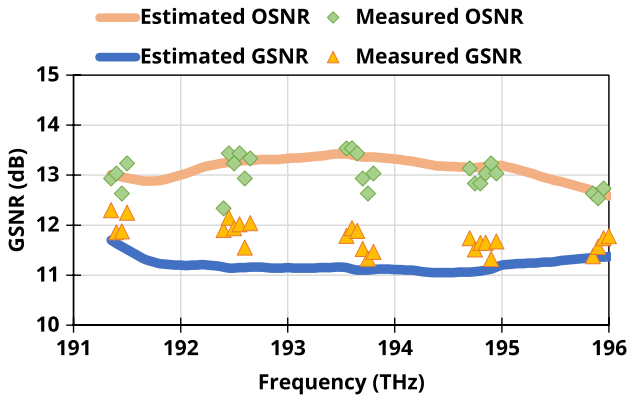

Fig. 7. Comparison of the measured and estimated OSNR and GSNR from PM-8QAM @ 2000 km.

B. Results

The validation demonstrates that the tool effectively predicts both the OSNR and the GSNR with excellent accuracy; in addition, it is able to accurately capture the frequency variation of both metrics. The first observed case is the 2000 km forward direction with PM-8QAM modulated CUTs, which is shown in Fig. 7. Both the OSNR and the GSNR are measured (diamond and triangular markers, respectively) and compared to the estimates (continuous lines). The OSNR was measured with an OSA, while the GSNR has been measured by reading the BER from the cards and inverting the B2B characteristic of each card, as discussed in Section 3. This first result demonstrates good accuracy in the estimates of both the OSNR and the GSNR. It can be noted that the estimated OSNR has an error within 0.4 dB, except two outliers at 192.4 THz and at 193.75 THz. In this case, GNPy shows an excellent capability to predict the frequency variation of the two metrics and a conservative estimation of the GSNR as expected by the GGN model, for which estimation of the NLI is worst case. Here, the discrepancy between the measured GSNR and the estimated one is within 1 dB.

Moreover, we performed a power sweep (i.e., we varied the transmitted power at the beginning of each optical line by a power offset from −3 dB up to +1 dB). Figure 8 shows the results of the power sweep as a comparison of the measured and the estimated GSNR for channels #2, #48, and #92—at 191.4 THz, 193.5 THz, and 195.9 THz—i.e., two at the edges and one in the middle of the spectrum, at 800 km, 1200 km, and 2000 km. The results show good accuracy in predicting the GSNR as well as the optimum power (i.e., the one maximizing the GSNR of the central channel), as shown by the local-optimum global-optimum (LOGO) approach [30]. The predicted optimum power is always within 0.5 dB of the measured optimum. This demonstrates the accuracy of the tool to estimate the optimum power; thus, it can be integrated into an optical controller to optimize the transmitted power.

Figures 9, 10, and 11 report the estimated GSNR (blue lines) and the measured one (orange dots) for all the investigated scenarios with the PM-8QAM, PM-QPSK, and PM-16QAM modulation formats, respectively. Each of them has been reported for several distances and for both directions. Furthermore, Fig. 12 reports the results when the Raman amplification is turned off. The QoT estimator shows good accuracy in the estimation, showing a small discrepancy with respect to the measured values and demonstrating a good capability when predicting the frequency variation of the GSNR. Moreover, as the QoT estimator is based on the GGN model, it neglects the impact of the modulation format on the NLI generation. For this reason, the QoT estimator predicts the same GSNR when only the modulation format changes. This assumption is validated because the modulation format has a negligible impact on the measured GSNR. Observing the shorter 400 km distances, in Figs. 9(a), 9(f), 11(a), and 11(d), a larger inaccuracy is present in the middle of the band. The error decreases when the distance is increased since the overall GSNR reduction mitigates the uncertainty on both the ASE

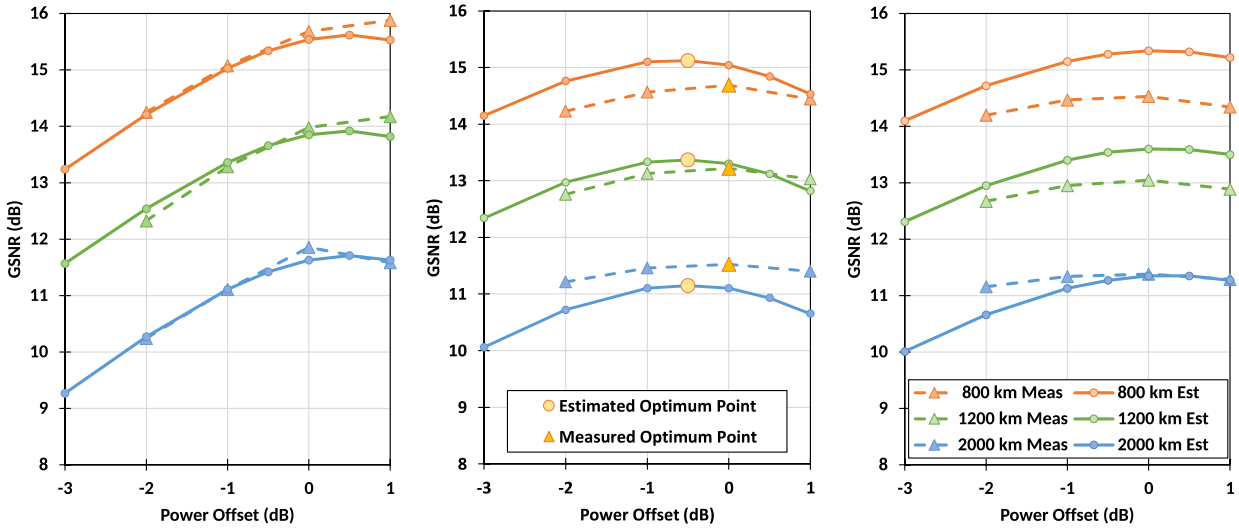

(a) Channel #2 at 191.4 THz. **(b)** Channel #48 at 193.5 THz. **(c)** Channel #92 at 195.9 THz.

Fig. 8. Comparison of the estimated and measured GSNR in a power sweep for PM-8QAM. The legend shown in (c) applies to all three graphs.

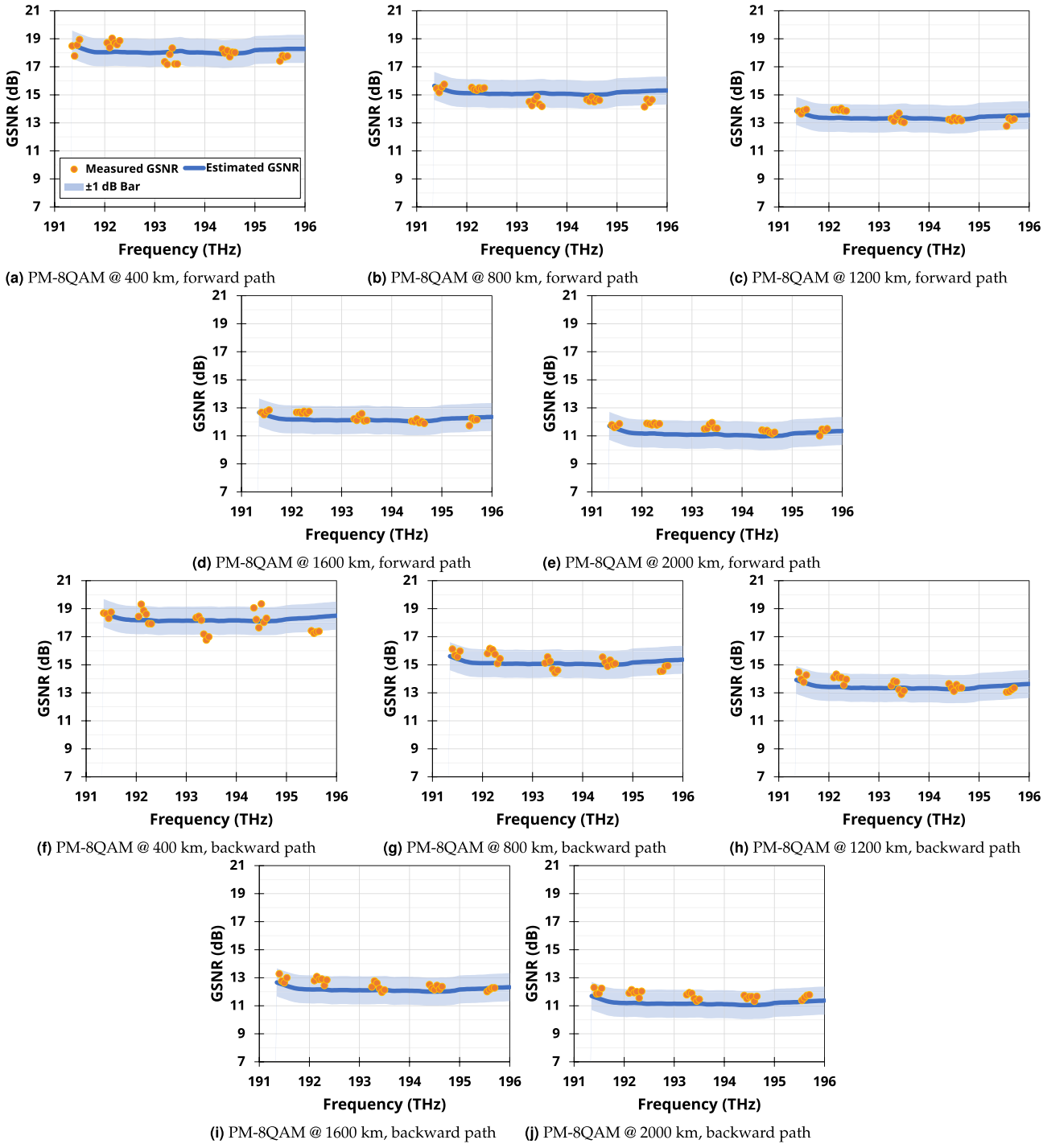

(a) PM-8QAM @ 400 km, forward path (b) PM-8QAM @ 800 km, forward path (c) PM-8QAM @ 1200 km, forward path

(d) PM-8QAM @ 1600 km, forward path (e) PM-8QAM @ 2000 km, forward path

(f) PM-8QAM @ 400 km, backward path (g) PM-8QAM @ 800 km, backward path (h) PM-8QAM @ 1200 km, backward path

(i) PM-8QAM @ 1600 km, backward path (j) PM-8QAM @ 2000 km, backward path

Fig. 9. Comparison of estimation with measurement for PM-8QAM.

noise and NLI. For shorter distances, in fact, it is more difficult to accurately measure the GSNR because i) the BER is lower, so it is less stable in the measurement time window (fewer errors are counted), and ii) the GSNR itself is higher and therefore more sensitive to small inaccuracies. For shorter distances, in fact, the noise power is smaller and thus, each inaccuracy has a larger effect on the overall GSNR. For the same reason, the B2B characterization also is less accurate where the BER is lower and the OSNR is higher, making the measurement less accurate.

Finally, the estimated GSNR shows excellent accuracy when the Raman cards are turned off, as shown in Fig. 12, demonstrating that the QoT estimator can also be used as an engine for what-if investigations in a techno-economic analysis to understand whether it is advantageous to use Raman amplifiers to improve the GSNR of a network.

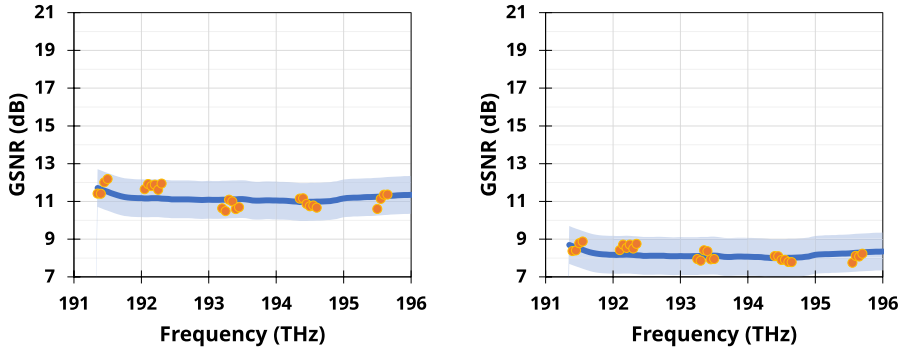

(a) PM-QPSK @ 2000 km, forward path **(b)** PM-QPSK @ 4000 km, loop-back

Fig. 10. Comparison of estimation with measurement for PM-QPSK.

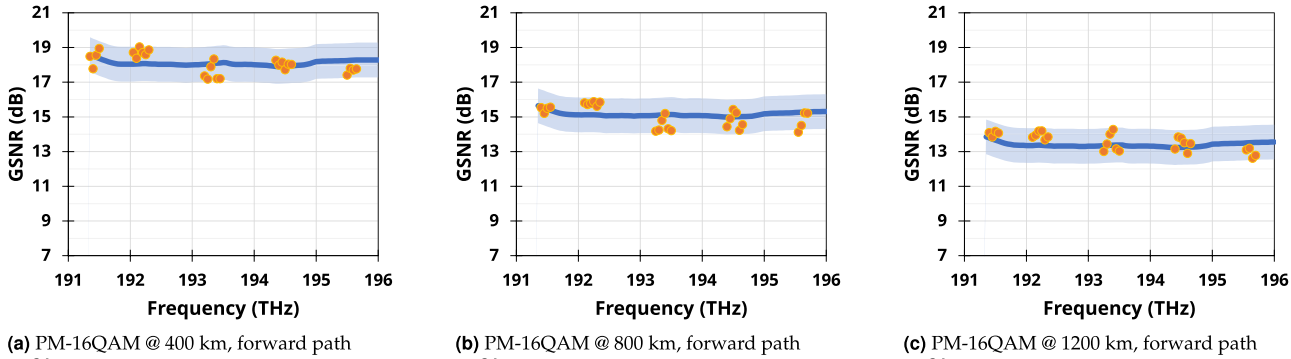

(a) PM-16QAM @ 400 km, forward path **(b)** PM-16QAM @ 800 km, forward path **(c)** PM-16QAM @ 1200 km, forward path

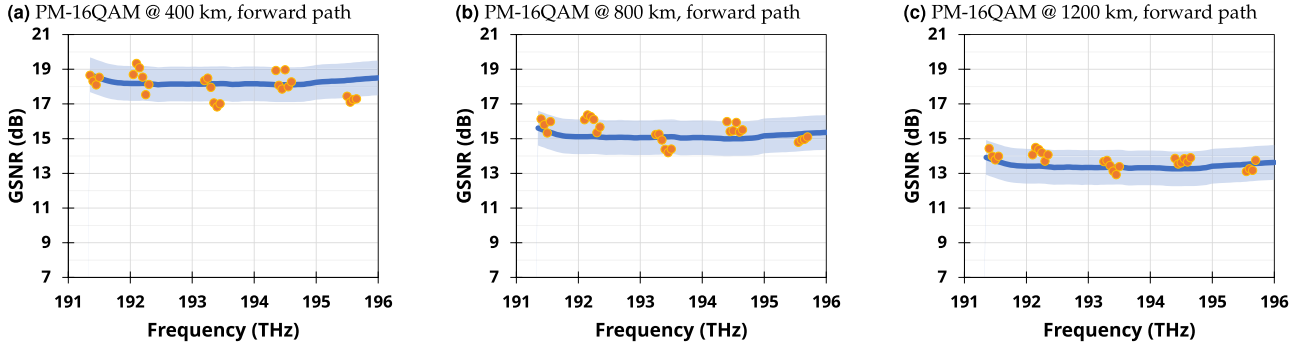

(d) PM-16QAM @ 400 km, backward path **(e)** PM-16QAM @ 800 km, backward path **(f)** PM-16QAM @ 1200 km, backward path

Fig. 11. Comparison of estimation with measurement for PM-16QAM.

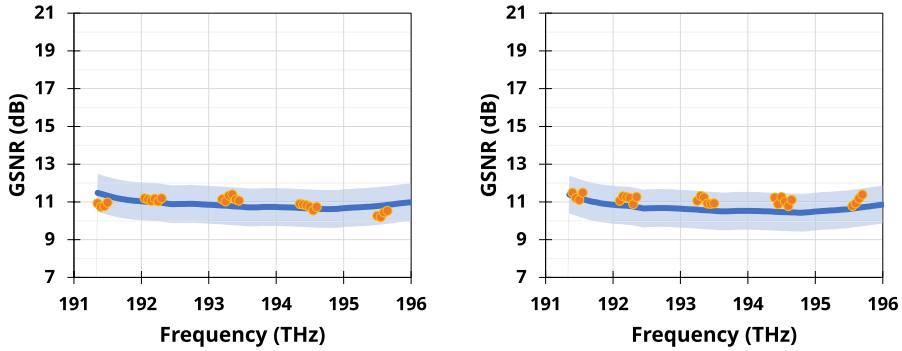

(a) PM-8QAM @ 2000 km, forward path **(b)** PM-8QAM @ 2000 km, backward path

Fig. 12. Comparison of estimation with measurement for PM-8QAM with Raman amplifiers turned off.

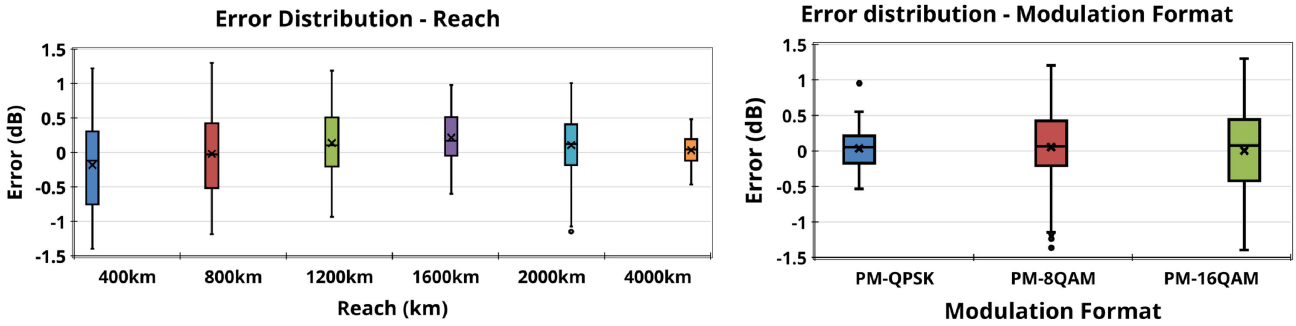

(a) Error distribution versus reach.

(b) Error distribution versus modulation.

Fig. 13. Error distribution with respect to the reach and the modulation format.

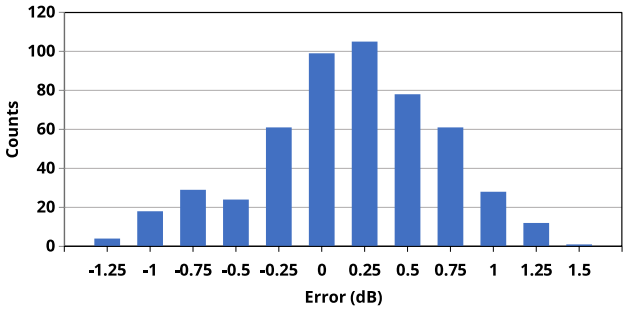

Fig. 14. Error histogram over all measured points.

Finally, the error of each channel in each scenario has been computed as the difference between the measured GSNR and the estimated GSNR (i.e., Measured GSNR–Estimated GSNR). This set of errors has more than 500 values. Figure 13(a) reports the error distribution for each distance and Fig. 13(b)] reports error distribution for each modulation format. The distributions looks quite symmetric with a positive offset of ∼0.25 dB. A total of ∼80% of the estimations are within 1 dB of error at 400 km. This percentage increases to ∼92% at 800 km, and it reaches 100% for larger distances. The largest error (1.4 dB) is at 400 km. This value decreases at larger distances, and all the errors are within 0.5 dB at 4000 km. The average and the median error is ∼0.5 dB at 400 km and 800 km; then it oscillates around 0.4 dB and 0.3 dB when the distance increases to 1200 km and 2000 km. Finally, the value shrinks down to 0.2 dB when the reach is 4000 km. The PM-QPSK exhibits the smallest error distribution, whereas PM-16QAM exhibits the largest inaccuracy. The average and the median error are roughly 0.2 dB for PM-QPSK, 0.4 dB for PM-8QAM, and 0.5 dB for PM-16QAM. This is because PM-QPSK has been measured at the largest distances, where the accuracy is better, while PM-16QAM has been probed at the shortest reaches of 400 km, 800 km, and 1200 km. Finally, Fig. 14 reports the error distribution. A total of 90% of the errors are smaller than 1 dB. Moreover, the distribution is not symmetric around 0; in fact, 74% of the errors are positive and the largest value is 1.4 dB. This means that most of the estimations are conservative. The error is due to three main factors: (i) the conservative assumptions on which the GGN model is based, (ii) the uncertainty in the measurement of the GSNR, and (iii) the inaccuracy in measuring the parameters provided to GNPy to compute the estimated GSNR. In particular, factors (ii) and (iii) can lead to a nonconservative estimation of the overall performances, even if the NLI model is conservative. Furthermore, we think that a critical parameter is represented by the input connector loss because its value has been assumed and it determines the amount of NLI introduced by each fiber span; thus, the estimated GSNR.

5. CONCLUSIONS AND NEXT STEPS

We presented GNPy for the physical layer abstraction of optical networks by describing the general structure, the functionalities, and its core structure, in addition to describing the scientific bases. Then we delineated the validation procedure of the QoT estimator, which can be, in general, followed by using GNPy on any real network to predict the QoT of a lightpath. Later, we described the testbed we used and compared the estimated GSNR against the measured values. We showed that, following a procedure that relies only on the data obtained by querying the network equipment and the data present in the equipment documentation, it is possible to obtain excellent accuracy. In our measurement, the error is within 1 dB in 90% of cases on a sample size of 500 measurements. Furthermore, we showed that GNPy is able to predict the optimum transmitted power with good accuracy—within 0.5 dB; thus, it can be used in an optical line controller to compute the optimum working point. This validation was carried out with excellent results by varying the paths' distances, the modulation format, and the network configuration, and by probing the C-band on different spectral areas to show the ability of the QoT estimator to predict the frequency variation of the GSNR. Moreover, the capability to track variations in the amplifier setup demonstrates that GNPy is suitable as an engine for a what-if framework. Then, an initial step in validating the accuracy in predicting the performance of Raman amplification has been demonstrated. Additional testing with a focus on longer fiber spans and even higher distribution of hybrid or Raman amplification will be a valuable source of test data. Another further step, so far missing, is a brown-field validation to test the accuracy in the presence of environmental and aging issues. In a brown-field scenario,

in fact, many splices are present along the fibers because of the continuous fiber cuts and the connectors may not be perfectly cleaned.

Acknowledgment. GNPy has been developed by the OOPT–PSE working group within the Telecom Infra Project.

REFERENCES

1. "TIP Open Optical & Packet Transport (OOPT)," https://telecominfraproject.com/oopt/.
2. "GitHub repository of GNPy," https://github.com/Telecominfraproject/oopt-gnpy.
3. V. Kamalov, M. Cantono, V. Vusirikala, L. Jovanovski, M. Salsi, A. Pilipetskii, D. K. M. Bolshtyansky, G. Mohs, E. R. Hartling, and S. Grubb, "The subsea fiber as a Shannon channel," in *Proceedings of SubOptic* (2019).
4. I. Busi and S. Belotti, "YANG model for requesting path computation," draft-IETF-TEAS-Yang-path-computation-06 (Internet Engineering Task Force, 2019).
5. V. Curri, A. Carena, A. Arduino, G. Bosco, P. Poggiolini, A. Nespola, and F. Forghieri, "Design strategies and merit of system parameters for uniform uncompensated links supporting Nyquist-WDM transmission," J. Lightwave Technol. **33**, 3921–3932 (2015).
6. A. Ferrari, M. Cantono, U. Waheed, A. Ahmad, and V. Curri, "Networking benefits of advanced DSP techniques and hybrid fiber amplification," in *19th International Conference on Transparent Optical Networks (ICTON)* (IEEE, 2017), pp. 1–4.
7. A. Ferrari, D. Pilori, E. Virgillito, and V. Curri, "Power control strategies in C+L optical line systems," in *Optical Fiber Communication Conference* (Optical Society of America, 2019), paper W2A48.
8. V. Curri, M. Cantono, and R. Gaudino, "Elastic all-optical networks: a new paradigm enabled by the physical layer. How to optimize network performances?" J. Lightwave Technol. **35**, 1211–1221 (2017).
9. B. D. Taylor, G. Goldfarb, S. Bandyopadhyay, V. Curri, and H.-J. Schmidtke, "Towards a route planning tool for open optical networks in the telecom infrastructure project," in *Optical Fiber Communication Conference* (Optical Society of America, 2018), paper Tu3E–4.
10. M. Filer, M. Cantono, A. Ferrari, G. Grammel, G. Galimberti, and V. Curri, "Multi-vendor experimental validation of an open source QoT estimator for optical networks," J. Lightwave Technol. **36**, 3073–3082 (2018).
11. A. Ferrari, M. Filer, K. Balasubramanian, Y. Yin, E. LeRouzic, J. Kundrát, G. Grammel, G. Galimberti, and V. Curri, "Experimental validation of an open source quality of transmission estimator for open optical networks," in *Optical Fiber Communication Conference and Exhibition (OFC)* (Optical Society of America, 2020), paper W3C.2.
12. J.-L. Auge, V. Curri, and E. L. Rouzic, "Open design for multi-vendor optical networks," in *Optical Fiber Communication Conference (OFC)* (Optical Society of America, 2019), paper Th1I.2.
13. J. Kundrát, O. Havliš, J. Jedlinský, and J. Vojtěch, "Opening up ROADMs: let us build a disaggregated open optical line system," J. Lightwave Technol. **37**, 4041–4051 (2019).
14. "Exchange with GNPy to check path feasibility," https://git.opendaylight.org/gerrit/c/transportpce/+/81785.
15. A. Ferrari, A. Tanzi, S. Piciaccia, G. Galimberti, and V. Curri, "Selection of amplifier upgrades addressed by quality of transmission and routing space," in *Optical Fiber Communication Conference and Exhibition (OFC)* (Optical Society of America, 2019), pp. 1–3.
16. M. Cantono, D. Pilori, A. Ferrari, C. Catanese, J. Thouras, J.-L. Augé, and V. Curri, "On the interplay of nonlinear interference generation with stimulated Raman scattering for QoT estimation," J. Lightwave Technol. **36**, 3131–3141 (2018).
17. M. Cantono, A. Ferrari, D. Pilori, E. Virgillito, J. Augé, and V. Curri, "Physical layer performance of multi-band optical line systems using Raman amplification," J. Opt. Commun. Netw. **11**, A103–A110 (2019).
18. I. Roberts, J. M. Kahn, J. Harley, and D. W. Boertjes, "Channel power optimization of WDM systems following Gaussian noise nonlinearity model in presence of stimulated Raman scattering," J. Lightwave Technol. **35**, 5237–5249 (2017).
19. D. Semrau, R. I. Killey, and P. Bayvel, "The Gaussian noise model in the presence of inter-channel stimulated Raman scattering," J. Lightwave Technol. **36**, 3046–3055 (2018).
20. J. Bromage, "Raman amplification for fiber communications systems," J. Lightwave Technol. **22**, 79–93 (2004).
21. A. Carena, G. Bosco, V. Curri, Y. Jiang, P. Poggiolini, and F. Forghieri, "EGN model of nonlinear fiber propagation," Opt. Express **22**, 16335–16362 (2014).
22. F. Zhang, Q. Zhuge, and D. V. Plant, "Fast analytical evaluation of fiber nonlinear noise variance in mesh optical networks," J. Opt. Commun. Netw. **9**, C88–C97 (2017).
23. R. T. Fielding and R. N. Taylor, "Architectural styles and the design of network-based software architectures," Doctoral dissertation (University of California, Irvine, 2000).
24. R. Enns, M. Bjorklund, J. Schoenwaelder, and A. Bierman, "Network Configuration Protocol (NETCONF)," IETF RFC 6241, 2011.
25. M. A. Taubenblatt, "Optical interconnects for high-performance computing," J. Lightwave Technol. **30**, 448–457 (2011).
26. A. Ferrari, M. Cantono, B. Mirkhanzadeh, Z. Lu, A. Shakeri, C. Shao, M. Tacca, M. Razo, A. Fumagalli, G. Martinelli, and G. M. Galimberti, "A two-layer network solution for reliable and efficient host-to-host transfer of big data," in *20th International Conference on Transparent Optical Networks (ICTON)* (IEEE, 2018), pp. 1–4.
27. D. Derickson, C. Hentschel, and J. Vobis, *Fiber Optic Test and Measurement* (Prentice Hall, 1998).
28. V. Curri and A. Carena, "Merit of Raman pumping in uniform and uncompensated links supporting NyWDM transmission," J. Lightwave Technol. **34**, 554–565 (2015).
29. D. J. Elson, G. Saavedra, K. Shi, D. Semrau, L. Galdino, R. Killey, B. C. Thomsen, and P. Bayvel, "Investigation of bandwidth loading in optical fibre transmission using amplified spontaneous emission noise," Opt. Express **25**, 19529–19537 (2017).
30. P. Poggiolini, G. Bosco, A. Carena, R. Cigliutti, V. Curri, F. Forghieri, R. Pastorelli, and S. Piciaccia, "The LOGON strategy for low-complexity control plane implementation in new-generation flexible networks," in *Optical Fiber Communication Conference and Exposition and the National Fiber Optic Engineers Conference (OFC/NFOEC)* (Optical Society of America, 2013), pp. 1–3.